Smad1 transcription factor integrates BMP2 and Wnt3a signals in migrating cardiac progenitor cells

Junfang Song[1,2], James McColl[1], Esther Camp[3], Niki Kennerley, Gi Fay Mok, Dominique McCormick, Timothy Grocott, Grant N. Wheeler, and Andrea E. Münsterberg[4]

School of Biological Sciences, University of East Anglia, Norwich Research Park, Norwich NR4 7TJ, United Kingdom

Edited by Clifford J. Tabin, Harvard Medical School, Boston, MA, and approved April 8, 2014 (received for review November 22, 2013)

In vertebrate embryos, cardiac progenitor cells (CPCs) undergo long-range migration after emerging from the primitive streak during gastrulation. Together with other mesoderm progenitors, they migrate laterally and then toward the ventral midline, where they form the heart. Signals controlling the migration of different progenitor cell populations during gastrulation are poorly understood. Several pathways are involved in the epithelial-to-mesenchymal transition and ingression of mesoderm cells through the primitive streak, including fibroblast growth factors and wingless-type family members (Wnt). Here we focus on early CPC migration and use live video microscopy in chicken embryos to demonstrate a role for bone morphogenetic protein (BMP)/SMA and MAD related (Smad) signaling. We identify an interaction of BMP and Wnt/glycogen synthase kinase 3 beta (GSK3β) pathways via the differential phosphorylation of Smad1. Increased BMP2 activity altered migration trajectories of prospective cardiac cells and resulted in their lateral displacement and ectopic differentiation, as they failed to reach the ventral midline. Constitutively active BMP receptors or constitutively active Smad1 mimicked this phenotype, suggesting a cell autonomous response. Expression of GSK3β, which promotes the turnover of active Smad1, rescued the BMP-induced migration phenotype. Conversely, expression of GSK3β-resistant Smad1 resulted in aberrant CPC migration trajectories. Derepression of GSK3β by dominant negative Wnt3a restored normal migration patterns in the presence of high BMP activity. The data indicate the convergence of BMP and Wnt pathways on Smad1 during the early migration of prospective cardiac cells. Overall, we reveal molecular mechanisms that contribute to the emerging paradigm of signaling pathway integration in embryo development.

live imaging | cell tracking

Cardiac progenitor cells (CPCs) are among the first cell lineages to be specified in vertebrate embryos. In avian embryos, prospective cardiac cells that have been fate-mapped to the mid- and anterior primitive streak at Hamburger Hamilton (HH) stage 3 form bilaterally symmetric heart-forming regions in the lateral mesoderm postgastrulation (1–4) and a wide arc of progenitors at HH5-7 (5). By HH10, a simple primary heart tube is formed by fusion of the bilateral progenitor cell populations at the ventral midline (6). The process of early heart formation is highly conserved in amniote embryos. Defects are often incompatible with successful development and can be lethal or may lead to a spectrum of congenital malformations. The underlying genetic or environmental causes of congenital heart defects are not understood in many cases (7).

Several pathways are involved in the initial specification of cardiac cells, including bone morphogenetic proteins (BMPs), fibroblast growth factors (FGFs), and wingless-type family members (Wnt). BMP2 (8-12) and FGF8 (13) are known to promote the specification of cardiac progenitors, whereas the Wnt/β-catenin pathway inhibits cardiac differentiation in mouse (14, 15), chick (16), and amphibian embryos (17). Conversely, noncanonical Wnt signaling is sufficient to induce cardiogenesis in amphibians (18), and an initial requirement for β-catenin-dependent Wnt signaling for mesoderm fate specification has also been identified. Thus, multiple Wnt pathways are involved at different stages to regulate cardiac morphogenesis and progenitor cell self-renewal (19, 20).

Here we do not primarily address cell fate specification, instead concentrating on the mechanisms involved in regulating migration behavior, which are still enigmatic. To address this and to observe cell movement directly, we developed long-term video microscopy to track individual GFP-labeled cells in live chicken embryos. We showed previously that positive and negative chemotaxis, mediated by FGF4 and FGF8, controls cell movement patterns of prospective paraxial and lateral plate mesoderm cells, which arise from the primitive streak at HH stage 4 (21). We also found that movement trajectories of cardiogenic progenitor cells ingressing at HH3 are controlled by Wnt3a signals. The response to Wnt3a depends on the small GTPase RhoA, suggesting effects on the actin cytoskeleton, and disruption of Wnt3a signaling leads to aberrant migration trajectories and cardia bifida (22).

After BMP-receptor-mediated C-terminal phosphorylation, active Smad1 associates with Smad4, a co-Smad, and translocates into the nucleus to regulate specific gene expression (reviewed in refs. 23 and 24). MAP kinases and glycogen synthase kinase

DEVELOPMENTAL BIOLOGY

Significance

Prospective cardiac cells emerge during gastrulation and undergo long-range migration toward the ventral midline, where they fuse to give rise to a single contractile tube, which subsequently undergoes complex morphogenesis. How cardiac progenitor cells are guided in their movement by extrinsic signals is still enigmatic. We previously identified wingless-type family member (Wnt) 3a as an important guidance signal. Here we used live video microscopy in chick embryos to uncover a role for bone morphogenetic proteins (BMPs) in the control of cardiac progenitor cell migration. Functional approaches, complementation, and rescue experiments reveal cooperation between BMP signalling and the Wnt/glycogen synthase kinase 3 beta pathway: both converge to stabilize activated SMA and MAD related protein. Insights into the molecular integration of signaling pathways in migrating cells affect our understanding of cardiac malformations during embryo development.

Author contributions: J.S., J.M., E.C., and A.E.M. designed research; A.E.M. directed the research; J.S., J.M., E.C., N.K., G.F.M., and D.M. performed research; T.G. contributed new reagents/analytic tools; J.S., J.M., E.C., G.N.W., and A.E.M. analyzed data; and J.M., T.G., G.N.W., and A.E.M. wrote the paper.

The authors declare no conflict of interest.

This article is a PNAS Direct Submission.

[1]J.S. and J.M. contributed equally to this work.

[2]Present address: Division of Cell and Developmental Biology, College of Life Sciences, MSI/Wellcome Trust Building, University of Dundee, Dundee DD1 5EH, United Kingdom.

[3]Present address: Department of Physiology, School of Medical Sciences, University of Adelaide, Adelaide, SA 5005, Australia.

[4]To whom correspondence should be addressed. E-mail: a.munsterberg@uea.ac.uk.

This article contains supporting information online at www.pnas.org/lookup/suppl/doi:10.1073/pnas.1321764111/-/DCSupplemental.

3 beta (GSK3β) kinase catalyze inhibitory phosphorylations in the Smad1 linker region. This restricts Smad1 activity and facilitates recognition by the ubiquitin ligase Smurf1 (SMAD ubiquitination regulatory factor 1), causing degradation or, alternatively, cytoplasmic retention (24–26).

Here we demonstrate a role for BMP/Smad signaling in the control of migration behavior and reveal a link between Wnt3a and BMP signaling in migrating CPCs. The data show that BMP and Wnt pathways converge on Smad1 to control movement behavior of prospective cardiac cells.

Results

BMP2 and BMP4, as well as their downstream effectors, Smad1 and Smad5, are expressed in the HH3-3$^+$ primitive streak when CPCs ingress. By stage HH6, BMP2 and BMP4 are expressed lateral to the heart fields (Fig. S1 and refs. 27 and 28; http://geisha.arizona.edu). A role of BMPs in the modulation of cell movement behavior has been demonstrated in cancer cell lines, monocyte chemotaxis, and axon guidance (29–31), as well as during the initiation of cardiac looping (32–34). Thus, we determined whether manipulation of BMP signaling activity would alter the migration behavior of prospective cardiac cells. A number of approaches were used, including implantation of growth factor-coated beads or cell pellets, or electroporation of expression plasmids into cardiogenic regions of the primitive streak at HH3 to HH3$^+$, followed by time-lapse imaging (Fig. 1 *A–D*), as described previously (22). To determine normal migration trajectories, we first imaged individual GFP-only expressing CPCs, tracked their final position, and determined their distance from the midline at HH9, when a primitive heart tube had formed (Fig. 1 *E–I*). As before, we confirmed normal cardiac morphology and differentiation of GFP-electroporated CPCs, using ventricular myosin heavy chain (vMHC) as a marker (22).

Next, we assessed the effect of beads soaked in BSA, recombinant BMP2 protein, or an implanted Wnt3a-secreting cell pellet on the path of migrating CPCs (Fig. 1 *J–L*). BMP2 beads implanted close to the HH3 primitive streak significantly altered the migration behavior and final position of cardiac progenitors (Fig. 1 *K* and *M*). At HH9, the majority of cells were found at a greater distance from the midline compared with the control side, where GFP-positive cells contributed to the forming heart tube (Fig. 1 *K* and Fig. S2). Beads coated in BSA did cause a physical barrier but did not affect the final position of CPCs (Fig. 1 *J* and *M* and Fig. S2). The effect of BMP2 was similar to the effect of Wnt3a-expressing cell pellets, which we reported previously (22). Increased levels of Wnt3a resulted in more pronounced lateral migration trajectories of CPCs, which at HH9 were found at a greater distance from the midline (Fig. 1 *L* and *M*). Therefore, to exclude the possibility that BMP2 beads affected the levels of known guidance signals, we performed in situ hybridization and found no evidence of ectopic expression of either Wnt3a or FGF-8 (Fig. S3).

Next, we sought to determine whether the lateral displacement of CPCs was a result of BMP2 having an effect on their early exit trajectories from the primitive streak. Individual GFP-expressing CPCs were imaged and tracked, and their initial exit trajectories were determined. To characterize the baseline for the initial exit trajectory experiments, GFP-expressing cell trajectories were analyzed by first determining the angle of each cell at each image point, with its origin at the midline as the reference point (for the first 60 min). Angles for each coordinate were calculated and then averaged to provide mean trajectory values, which were

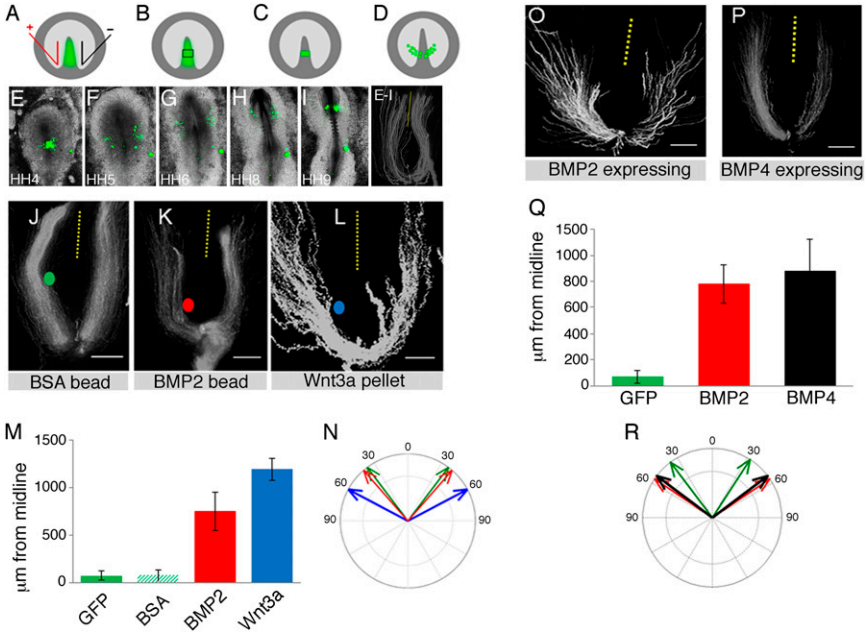

Fig. 1. BMP2 alters CPC migration patterns. *(A–D)* Experimental schematic. *(A)* CPC-producing regions of the HH3 primitive streak were GFP electroporated, *(B* and *C)* grafted into stage-matched embryos, *(D)* recorded by time-lapse microscopy, and had their tracks visualized by image processing. *(E–I)* Time-lapse microscopy of GFP-expressing cells overlaid on white-light images. Trajectories for GFP-only-expressing CPCs. *(J–L)* BSA (green) and BMP2 (red) beads and Wnt3a (blue) cell pellets were grafted into the CPC migration path. Final distance from the midline (dotted lines to center of trajectories) and initial exit trajectories angles were determined. (Scale bars, 500 μm.) *(M)* Final distance from the midline (μm) for the experimental conditions indicated. Errors are standard deviations. *(N)* Initial exit trajectories for different experimental conditions; colors correspond to experimental conditions in *J–L*. Errors are standard error of the mean, denoted by the width of the arrows. *(O–P)* CPC-producing regions of the HH3 primitive streak were electroporated with pCAβ-IRES-GFP vector so that they expressed either BMP2 or BMP4 and GFP, grafted into stage-matched embryos, and had their tracks recorded. (Scale bars, 500 μm.) *(Q)* Final distance from the midline, BMP2 and BMP4 expressing. Errors are standard deviations. *(R)* Initial exit trajectories, BMP2 and BMP4 expressing. Errors are standard error of the means, denoted by the width of the arrows.

plotted in histograms to generate compass plots. For control GFP-labeled cells, the mean angle at which CPCs initially migrate for all trajectories is 37° ± 2° (Fig. 1*N*). Early exit trajectories on the BMP2 bead side of the embryo aligned well with the initial migration angle of cells exposed to BSA beads or of control GFP-labeled cells, but trajectories did alter after cells had encountered the bead. In contrast, when Wnt3a-secreting pellets were implanted, they induced wider early exit trajectories compared with GFP-labeled CPCs (Fig. 1*N*). Both the Wnt3a pellets and the BMP2 beads were placed into the same position relative to the HH3 primitive streak and migrating CPCs (Fig. S4), but Wnt3a cell pellets affected CPCs on both sides of the embryo, in contrast to BMP2 beads, which only affected cells in close proximity. It is currently not clear whether this difference may be a result of the different means of ligand delivery.

To corroborate the bead experiments, we electroporated either chicken β-actin promoter (pCAβ)-BMP2-internal ribosomal entry site (IRES)-GFP or pCAβ-BMP4-IRES-GFP expression plasmid into cardiogenic regions of the primitive streak at HH3 to HH3^{+}. Time-lapse recordings showed that migration patterns of CPCs were significantly altered and that both BMP2- and BMP4-expressing progenitors displayed a more pronounced lateral migration route (Fig. 1 *O* and *P*). Many cells were found at a greater distance from the midline (Fig. 1*Q*) in extraembryonic or anterior lateral mesoderm, and they did not contribute to the primary heart tube and had wider exit trajectories (Fig. 1*R* and Table S1). However, we detected ectopic vMHC expression, illustrating that a proportion of the displaced prospective cardiac cells was still correctly specified (Fig. S5 *A* and *B*; $n = 3/7$). We note that the same effects on cell behavior (i.e., exit trajectory and final position from the midline) were observed for constitutively active forms of type 1 receptor overexpression (Fig. S6). In contrast, pCAβ-BMP2-IRES-GFP expression in paraxial mesoderm progenitors did not affect their migration trajectory or final position, although it inhibited somite epithelialization (Fig. S7, white arrows). The latter is consistent with published findings that elevated levels of BMP2 interfere with this process (8). This result suggested that different mesoderm progenitors respond differently to the same signals; however, in the following experiments, we focus on examining the response of CPCs. In all conditions in which aberrant migration trajectories were induced, overall embryonic development was the same as in control GFP-electroporated embryos (Fig. 1 *E–I*) or control bead-implanted embryos (Fig. S2). The anterior intestinal portal was generated, and the heart was formed (Figs. S2 and S5 *C–E*).

Our experiments revealed that both Wnt3a and BMP2/4 altered migration trajectories of CPCs as soon as they exited from the primitive streak (Fig. 1 *N* and *R*). In addition, the cells' response was cell autonomous. To determine how these different extracellular cues are integrated by CPCs, we examined the transcription factor Smad1, which becomes activated by BMP receptor-mediated C-terminal phosphorylation (Fig. 2*A*). First we set out to investigate effects on the distribution of active Smad protein. To do this, we grafted a BMP2 bead into cardiogenic mesoderm at HH5, fixed the samples, and immunolabeled them using an antibody that detects nuclear phospo-Smad1/5/8 (Fig. 2 *B–E*). A cross-section through nonimplanted embryos suggests that phosphorylated Smad1/5/8 levels remain constant across both the ectoderm and mesoderm, with the levels falling in the endoderm (Fig. 2 *C* and *D*). However, after implantation of a BMP2 bead, the levels of phospho-Smad were elevated close to the bead (at a distance of 50 μm from the bead; Fig. 2*E*), with the greatest increase being observed in the mesoderm (Fig. 2*F*). Analyzing only the mesoderm by integrating the intensity of concentric rings radiating out from the bead (Fig. 2*G*) revealed a graded increase of phospho-Smad levels proximal to the grafted bead (Fig. 2*H*). We performed a similar analysis after implanting Wnt3a-expressing cell pellets, which also led to

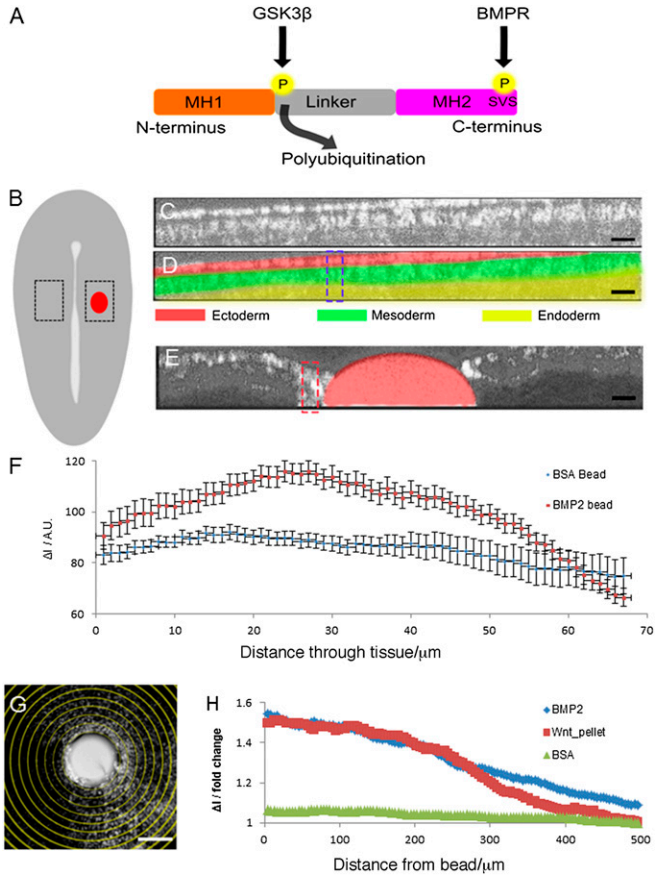

Fig. 2. Active forms of Smad1 alter CPC migration trajectories. *(A)* Schematic representation of Smad, indicating C terminus Ser-Ser-X-Ser motif. *(B)* Schematic showing where HH5 embryos were grafted with BSA, BMP2 beads, or a Wnt3a pellet and immunostained for phospho-Smad. Regions indicated by dotted lines were imaged using multiphoton microscopy. *(C–E)* Phospho-Smad distribution through the *z* axis of the tissue. *(C)* Raw data for nonbead region *(D)* annotated image showing ectoderm, mesoderm, and endoderm and (*E*) BMP2 bead region. (Scale bars, 50 μm.) *(F)* Phospho-Smad gradient through the *z* axis close to the bead (within 50 μm) for both the BMP2 bead ($n = 6$) and nonbead ($n = 4$) regions. Errors are standard error of the mean. *(G)* Averaged image for mesoderm region; images were analyzed by integrating the pixel intensity for concentric rings moving out from the center of the bead. (Scale bar, 100 μm.) *(H)* Change in phosphor-Smad intensity, with distance from bead for BSA, BMP2 beads, or a Wnt 3a pellet. Errors are standard error of the mean.

an increase in the levels of phospo-Smad1/5/8 in the mesoderm (Fig. 2*H*). For implanted BMP2 and Wnt3a pellets, phospho-Smad1/5/8 levels were 1.5-fold higher than background proximal to the bead, reducing to background levels over ∼500 μm. After implantation of BSA beads, the levels of nuclear phospho-Smad1/5/8 levels did not differ from background regions (Fig. 2*H*).

Our data suggest that BMP2 and Wnt3a pathways cooperate to guide CPC migration (Fig. 3*A*). To investigate this, we asked whether overexpression of wild-type or C-terminal phosphomimetic Smads would affect migrating cardiac progenitors (Fig. 3 *B–E*). Expression of wild-type Smad1 had no significant effect on migration, with the final position of CPCs from the midline not significantly different from those of control cells (Fig. 3*B*). These cells initially exited from the midline at an angle comparable with GFP-labeled controls (42° ± 2°) (Fig. 3*F*). However, electroporation of a constitutively active phosphomimetic form of Smad1, Smad1-EVE, in which the C-terminal serine phosphorylation sites were altered (Ser-Val-Ser to Glu-Val-Glu), resulted in initially wider trajectories of 59° ± 4° and an increased final

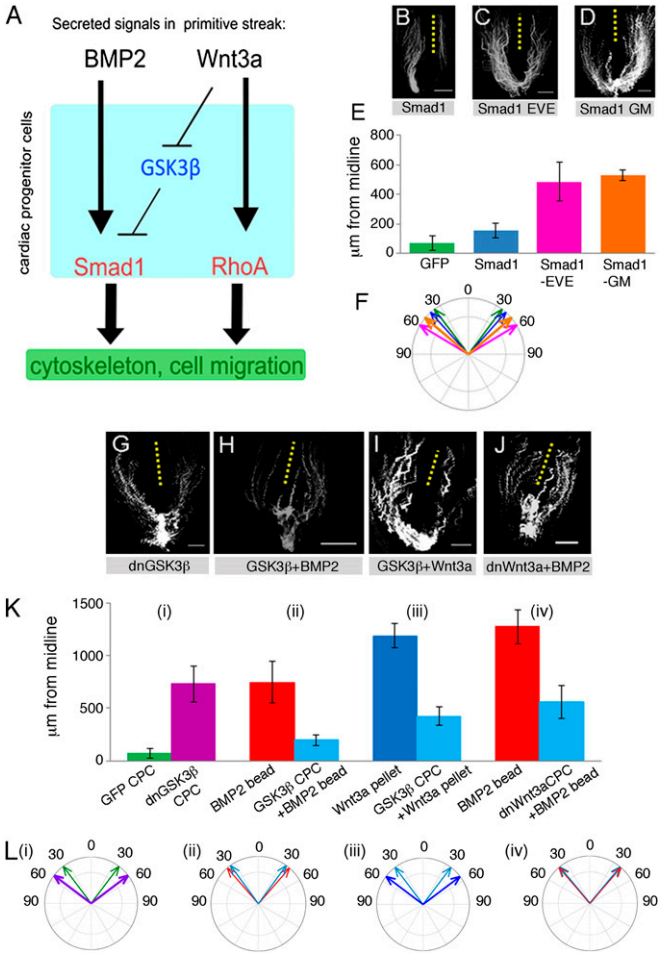

Fig. 3. *(A)* Schematic of BMP and Wnt3a cooperation. *(B–D)* Migration patterns for Smad variants. (Scale bars, 500 μm.) *(E)* Final distance from the midline, Smad variants. Errors are standard deviation. *(F)* Initial exit trajectories, Smad variants. Errors are standard error of the mean denoted by the width of the arrows. *(G–J)* migration patterns for electroporated cells expressing either dnGSK3β and GFP or recovery constructs, GSK3β, and dnWnt3a challenged with either BMP2 beads or Wnt3a pellets. (Scale bars, 500 μm.) *(K)* Final distance from the midline. Recovery construct expressing data are shown alongside control, (*i*) GFP-only-expressing cells compared with dnGSK3β-expressing cells, (*ii*) BMP2 bead plus GFP-expressing cells or plus GSK3β-expressing cells, (*iii*) Wnt3a pellet plus GFP-expressing cells or plus GSK3β-expressing cells, (*iv*) BMP2 bead plus GFP-expressing cells or plus dnWnt3a expressing cells. Errors are standard deviation. *(L)* Initial exit trajectories for recovery variants (*i–iv*) correspond to the treatments in *K*, *i–iv*. Errors are standard error of the mean, denoted by the width of the arrows.

distance from the midline (Fig. 3 *C*, *E*, and *F*). Smad1-EVE-GFP-positive cells that had moved into the lateral plate mesoderm during the migration process subsequently failed to contribute to the primary heart tube.

Active Smad1 is turned over after GSK3β-mediated phosphorylation in the linker region (Fig. 2*A*), which may explain why targeted misexpression of wild-type Smad1 had no significant effect on CPC migration. To address this possibility, we next examined the effect of a GSK3β-phosphorylation-resistant mutant, Smad1-GM (25). Cells electroporated with Smad1-GM were also found at an increased distance from the midline compared with GFP control cells and exhibited wider exit trajectories of 50° ± 4° (Fig. 3 *D–F*). Thus, application of either BMP2 or Wnt3a led to elevated phospho-Smad1/5/8 levels in cardiogenic mesoderm, raising the possibility that Wnt3a inhibition of GSK3β stabilizes activated Smad1/5/8 in migrating CPCs. These data indicate that activating Smad1 via BMP-type 1 receptor signaling or inhibiting Smad1 turnover, which is mediated by GSK3β phosphorylation, affects migration trajectories of cardiac progenitors.

To confirm the role of GSK3β in CPC migration, we carried out rescue experiments to recover the wider migration trajectories (Fig. 3 *G–J*). First, we expressed a dominant negative (dn) GSK3β mutant lacking the kinase domain, pCAβ-GSK3βKM-IRES-GFP, in CPCs. This led to both wider final positions from the midline (Fig. 3 *G* and *K, i*) and altered initial exit trajectories to 53° ± 4° (Fig. 3 *L, i*). This was similar to the GSK3β kinase-resistant Smad1 mutant (Fig. 3 *D–F*), consistent with the idea that GSK3β-mediated phosphorylation promotes Smad1 turnover in BMP-responsive cardiac progenitors. To further validate this notion, we examined whether wild-type GSK3β could inhibit the cells' response to a BMP2 bead. CPCs exposed to BMP2 beads displayed abnormal trajectories and were found further from the midline at HH9 (Fig. 1 *K* and *M*). Expression of wild-type GSK3β in cardiac progenitors inhibited the response to BMP2 beads, with the cells found close to the midline at similar distances compared with the control side (Fig. 3 *H* and *K, ii*). The angles of exit trajectories were very similar to those of control GFP cells (Fig. 3 *L, i*) and cells exposed to BMP2 beads (Fig. 3 *L, ii*).

We previously showed that Wnt3a guides CPC migration and that increased Wnt3a activity leads to wider movement trajectories and high frequency of cardia bifida (22). In this work, we provided evidence that the response to Wnt3a involved chemorepulsion and required RhoA activity. However, Wnt3a is also known to inhibit GSK3β. Thus, we asked whether overexpression of GSK3β in CPCs could block their response to Wnt3a. Time-lapse imaging and distance measurements showed that this was the case (Fig. 3 *I* and *K, iii*) compared with the effects of a Wnt3a pellet on GFP-labeled CPCs, which led to a wider migration trajectory (Fig. 3 *L, iii*). Therefore, GSK3β expression rescued altered CPC migration trajectories in response to both BMP2 and Wnt3a, indicating that Wnt signaling may cooperate with BMP2 signaling to control CPC migration via GSK3β and Smad1 (Fig. 3*A*).

Finally, expression of a dnWnt3a in migrating CPCs inhibited their response to a BMP2 bead. HH3 cardiogenic cells were electroporated with a dnWnt3a expression plasmid (22) (pCAβ-dnWnt3a-IRES-GFP), and their movement trajectories were recorded in the presence of a BMP2 bead implanted on one side (Fig. 3*J*). Movement trajectories were similar on both sides, and measurements at HH9 showed that when challenged with a BMP2 bead, dnWnt3a-expressing CPCs were closer to the midline than GFP control cells (Fig. 3 *K, iv*), and exit trajectories were very similar to those of GFP-only cells (Fig. 3 *L, iv*). Together, these data suggest that blockade of endogenous Wnt3a signaling abrogates the BMP response and support the hypothesis that endogenous Wnt3a is required to stabilize BMP signaling.

Discussion

Here we identify signaling cross-talk as a novel mechanism for controlling movement behavior and show that prospective cardiac cells respond to BMP2 cell-autonomously. Implanting BMP2 beads or BMP2 overexpression in migrating CPCs in vivo (Fig. 1 *K*, *O*, and *P*) led to their wider dispersal (Fig. 1 *M* and *Q*). This was phenocopied by constitutively active BMP receptors (Fig. S6) or active forms of Smad1 (Figs. 2*A* and 3 *C–F*). The effects of BMP or Wnt3a on CPC migration were rescued by overexpression of GSK3β. In addition, both these signals lead to increased phospho-Smad1/5/8 in cardiogenic mesoderm (Fig. 2 *F* and *H*). Therefore, we propose a model for BMP2/Wnt3a regulating early CPC migration trajectories via Smad1 phosphorylation (Fig. 3*A*). Whether RhoA acts in a parallel pathway or is an effector downstream of Smad1 is unclear at present.

It remains to be determined how BMP2 affects the directed migration of CPCs. We propose that BMP signaling repulses cardiac precursors in gastrula-stage embryos, initially away from the streak and, by HH6, back toward the midline. This would be consistent with the expression of BMP at these stages [Fig. S2 (8); http://geisha.arizona.edu]. It is possible, for example, that cells migrate along a gradient of decreasing BMP (HH4, HH5). The response of HH3 CPC explants to BMP2 beads corroborates this idea. CPCs avoid a BMP2 bead (Fig. S8 and Movies S1 and S2); however, the molecular mechanism remains to be established. The chemotactic potential of BMPs was first described in cell culture systems in which recombinant human BMP-2B (rhBMP-2B) induces the directed migration of human blood monocytes (29). It has also been observed in commissural neurons (31). Our previous work suggests that FGF8 and Wnt3a elicit a chemotactic response in CPCs (22), suggesting a mechanism by which FGF8, Wnt3a, and BMP2 may collectively result in guided cell migration during early cardiogenesis; for example, by generating morphogen gradients. Little is known about how signaling gradients control cell polarities by acting as global cues, but it has been shown that a Wnt5a signaling gradient controls limb elongation by establishing PCP in chondrocytes through Vangl2 (35). Our results show that Wnt3a-producing cell pellets affect CPC exit trajectories and the final distance from the midline on both sides. This is in contrast to BMP2 beads, which affect CPCs once they are in close proximity (Fig. 1 *K*, *L*, and *N*). It is unclear whether this difference may be a result of the different delivery methods of the ligands. The long-range distribution of lipid-modified Wnt proteins may be achieved through the formation of multimeric complexes and/or specialized filopodia (36). In other systems, other proteins aid Wnt protein distribution, such as surface Swim proteins (37) or heparan sulfate proteoglycans (38). Whether similar mechanisms are involved during the guidance of mesoderm progenitor migration remains to be established. At this time, it is not possible to image and track Wnt3a directly, and thus we cannot categorically rule in or rule out the possibility of Wnt3a acting as a long-range or short-range signal in our system.

BMPs are involved in cell polarity and migration at both the transcriptional and nontranscriptional levels (39). For example, it has been shown that BMP2 enhances the motility of prostate cancer cells via activation of integrins (30) and affects actin cytoskeleton reorganization and cell migration through regulation of phosphatidylinositide 3-kinase and cell division control protein 42 activity (40). Effects on LIM kinase 1 (LIMK), a key regulator of actin dynamics, which phosphorylates and inactivates cofilin, an actin depolymerizing factor, have also been reported (41, 42). Our results suggest that the activity of Smad1 is sufficient to alter CPC migration trajectories. Targeted misexpression of Smad1 had no effect on migration, suggesting that the quantity of Smad1 is not limiting; rather, its posttranslational modification by BMP and Wnt activity is crucial. We propose that Smad1 regulates components required for the migration process, such as cytoskeletal components, regulators of cytoskeletal dynamics, or cell adhesion molecules (43). It also has been shown that Smad1 linker phosphorylation mediated by cyclin-dependent kinases (CDK)8/9, which are components of transcriptional mediator and elongation complexes, facilitates efficient transcription of BMP target genes (44). Thus, it will be interesting to determine the possible role of this phosphorylation event for CPC behavior.

In the context of later heart development, high-resolution imaging in zebrafish has identified a role for BMPs during heart tube rotation; here, asymmetric BMP signaling differentially affects migratory behavior on one side (32–34). These latter observations, together with our data, implicate BMP signaling in early CPC migration and in cardiac morphogenesis in anamniotes and amniotes, respectively.

We show here that BMP2 expression in CPCs at HH3/3$^+$ resulted in the aberrant migration and lateral displacement of these progenitors. A subset of the displaced prospective cardiac cells was still able to express cardiac differentiation marker vMHC (Fig. S5 *A* and *B*). This indicates that expression of BMP2 can alter migration trajectory without necessarily affecting fate. However, it is likely that the final position the cells find themselves in is important for their differentiation, which depends on additional signals, such as FGF8 (13). Previous reports demonstrated ectopic expression of the homeobox-containing transcription factor Nkx2-5 and the zinc-finger transcription factor GATA-4 after implantation of BMP2-producing cells in gastrulating chicken embryos, and it was proposed that BMP-2 resulted in ectopic cardiac mesoderm specification (8). Our real-time observations indicate that in these experiments, cardiac progenitor cell migration may also have been affected. Effects of BMPs on progenitor cell migration in addition to effects on fate acquisition are also consistent with observations in genetically altered mice. For example, the conditional deletion of BMP receptor type 1a using mesoderm posterior 1, which acts in cardiogenic progenitors, results in the absence of the entire cardiac crescent and the restricted expression of myocardial progenitor markers Nkx2-5 and LIM homeobox 1 transcription factor (Isl1) to a small remaining cardiac field (9). Interestingly, these authors also showed that sustained activation of β-catenin signaling led to increased Isl1 expression but inhibited heart tube formation at the eight-somite stage. This would be consistent with the effects of Wnt3a on CPC migration reported here.

BMP signaling has well-known effects on cell fate determination during gastrulation, including on the induction of cardiac precursors (8–12). Thus, we cannot exclude the possibility that BMP overexpression produces changes in cell identity, and altered migration patterns could be a consequence of this. At present, we have no evidence that BMP2-overexpressing cells, which display altered exit trajectories from the streak, activate more lateral/posterior cell fates, such as blood (Fig. S9). However, it is difficult to know what a relevant marker for a possible change in fate might be. The answer to this question will require identification of Smad1 targets in early mesoderm progenitors, including CPCs.

Here we take the first step to dissect the signaling components required for the control of progenitor cell migration and uncovered cooperation between Wnt/GSK3β and BMP/Smad pathways. Previous findings demonstrated that Wnt/GSK3β signals through the stabilization of BMP/Smad during cell fate specification, both in neuroepidermal patterning (25) and, more recently, the induction of the retinal pigment epithelium (45). Future experiments will need to determine whether and how these pathways act to coordinate cell migration with cell fate specification.

Materials and Methods

Embryo Culture, Manipulations, and ex Vivo Migration Assay. Fertile brown eggs (Henry Stewart) were incubated at 38 °C in a humidified incubator. After embryos had reached appropriate stages, easy culture was prepared (46, 47). Electroporation, grafting, and ex vivo migration essays were carried out as described previously (21, 22, 48). Heparin beads (Sigma, H5263) were incubated with BMP2 (200 μg/mL; R&D Systems) or BSA (Promega) for 1 h before implantation, transferred with forceps to the ventral sides of host embryos, and implanted in the CPC migration path. Rescued embryos were always compared with control embryos, which used beads soaked in the same batch of ligand.

Long-term Video Microscopy. Embryos cultured in six-well cell culture plates (Falcon) were time-lapse-imaged on an inverted wide-field microscope (Axiovert; Zeiss). Brightfield and fluorescent images were captured every 6 min for 20–24 h, using Axiovision software. At the end of the incubation, most embryos had reached stage HH9 or HH10.

Tracking and Image Analysis. Automated fluorescent cell tracking was carried out using Optimas VI or Image-Pro (MediaCybernetics) software, as described (21, 22, 48). To quantify the effects observed, we measured the distance of GFP-labeled CPCs from the midline at the level of the forming heart at HH9, using Axiovision (Carl Zeiss), and confirmed statistical significance using Student *t* test ($P < 0.05$). For initial migration angle determination, the angle of each Cartesian coordinate for each time was calculated from the midline of the image, and the mean track angle was determined from the first 10 coordinates. All track angles were then plotted as compass plots (Matlab 2012b; Mathworks).

Plasmid Constructs and in Situ Hybridization. Expression constructs were generated in the pCAβ-IRES-GFP vector. Constitutively active receptor mutants of human activin-like kinase 3 (Q233D) and mouse activin-like kinase 6 (Q203D) were kindly provided by Andrew Chantry (University of East Anglia, Norwich). The constitutively active human SMAD1-EVE and the GSK3βKM kindly provided by Eddie DeRobertis (University of California, Los Angeles) are described in ref. 25. Wnt3a and dnWnt3a plasmid were described previously, and all plasmids were prepared for electroporation, as reported in ref. 22.

Cryosections and Immunochemistry. Embryos were embedded in optimal cutting temperature embedding medium (Tissuetek) and sectioned at 10-μm thickness on a Leica CM1900 cryostat. Immunochemistry was performed as described (22), using Rabbit anti-GFP (Abcam, 1:500) and mouse anti-rabbit-Alexa488 (Invitrogen, 1:1,000).

ACKNOWLEDGMENTS. We thank Paul Thomas for expert assistance in the Henry Wellcome Laboratory for Cell Imaging and Eddy DeRobertis and Andrew Chantry for plasmids. J.S., J.M., and E.C. were funded by British Heart Foundation project Grants PG/21821, PG/26150, and PG/29292 (to A.E.M). N.K. was funded by a Biotechnology and Biological Sciences Research Council (BBSRC) Doctoral Training Programme studentship, G.F.M. was funded by BBSRC project Grant BB/K003435 (to A.E.M.), and D.M. was funded by a British Heart Foundation studentship (FS/28379).

1. Garcia-Martinez V, Schoenwolf GC (1993) Primitive-streak origin of the cardiovascular system in avian embryos. *Dev Biol* 159(2):706–719.
2. Yutzey K, Gannon M, Bader D (1995) Diversification of cardiomyogenic cell lineages in vitro. *Dev Biol* 170(2):531–541.
3. Camp E, Münsterberg A (2011) Ingression, migration and early differentiation of cardiac progenitors. *Front Biosci (Landmark Ed)* 16:2416–2426.
4. Camp E, Dietrich S, Münsterberg A (2012) Fate mapping identifies the origin of SHF/AHF progenitors in the chick primitive streak. *PLoS ONE* 7(12):e51948.
5. Cui C, et al. (2009) Dynamic positional fate map of the primary heart-forming region. *Dev Biol* 332(2):212–222.
6. Redkar A, Montgomery M, Litvin J (2001) Fate map of early avian cardiac progenitor cells. *Development* 128(12):2269–2279.
7. Shieh JT, Srivastava D (2009) Heart malformation: What are the chances it could happen again? *Circulation* 120(4):269–271.
8. Andrée B, Duprez D, Vorbusch B, Arnold HH, Brand T (1998) BMP-2 induces ectopic expression of cardiac lineage markers and interferes with somite formation in chicken embryos. *Mech Dev* 70(1-2):119–131.
9. Klaus A, Saga Y, Taketo MM, Tzahor E, Birchmeier W (2007) Distinct roles of Wnt/beta-catenin and Bmp signaling during early cardiogenesis. *Proc Natl Acad Sci USA* 104(47):18531–18536.
10. Lee KH, Evans S, Ruan TY, Lassar AB (2004) SMAD-mediated modulation of YY1 activity regulates the BMP response and cardiac-specific expression of a GATA4/5/6-dependent chick Nkx2.5 enhancer. *Development* 131(19):4709–4723.
11. Schlange T, Andrée B, Arnold HH, Brand T (2000) BMP2 is required for early heart development during a distinct time period. *Mech Dev* 91(1-2):259–270.
12. Schultheiss TM, Burch JB, Lassar AB (1997) A role for bone morphogenetic proteins in the induction of cardiac myogenesis. *Genes Dev* 11(4):451–462.
13. Alsan BH, Schultheiss TM (2002) Regulation of avian cardiogenesis by Fgf8 signaling. *Development* 129(8):1935–1943.
14. Lickert H, et al. (2002) Formation of multiple hearts in mice following deletion of beta-catenin in the embryonic endoderm. *Dev Cell* 3(2):171–181.
15. Zhu W, et al. (2008) IGFBP-4 is an inhibitor of canonical Wnt signalling required for cardiogenesis. *Nature* 454(7202):345–349.
16. Marvin MJ, Di Rocco G, Gardiner A, Bush SM, Lassar AB (2001) Inhibition of Wnt activity induces heart formation from posterior mesoderm. *Genes Dev* 15(3):316–327.
17. Schneider VA, Mercola M (2001) Wnt antagonism initiates cardiogenesis in Xenopus laevis. *Genes Dev* 15(3):304–315.
18. Pandur P, Läsche M, Eisenberg LM, Kühl M (2002) Wnt-11 activation of a non-canonical Wnt signalling pathway is required for cardiogenesis. *Nature* 418(6898):636–641.
19. Tzahor E (2007) Wnt/beta-catenin signaling and cardiogenesis: Timing does matter. *Dev Cell* 13(1):10–13.
20. Cohen ED, Tian Y, Morrisey EE (2008) Wnt signaling: An essential regulator of cardiovascular differentiation, morphogenesis and progenitor self-renewal. *Development* 135(5):789–798.
21. Yang X, Dormann D, Münsterberg AE, Weijer CJ (2002) Cell movement patterns during gastrulation in the chick are controlled by positive and negative chemotaxis mediated by FGF4 and FGF8. *Dev Cell* 3(3):425–437.
22. Yue Q, Wagstaff L, Yang X, Weijer C, Münsterberg A (2008) Wnt3a-mediated chemorepulsion controls movement patterns of cardiac progenitors and requires RhoA function. *Development* 135(6):1029–1037.
23. Kretzschmar M, Doody J, Massagué J (1997) Opposing BMP and EGF signalling pathways converge on the TGF-beta family mediator Smad1. *Nature* 389(6651):618–622.
24. Shi Y, Massagué J (2003) Mechanisms of TGF-beta signaling from cell membrane to the nucleus. *Cell* 113(6):685–700.
25. Fuentealba LC, et al. (2007) Integrating patterning signals: Wnt/GSK3 regulates the duration of the BMP/Smad1 signal. *Cell* 131(5):980–993.
26. Sapkota G, Alarcón C, Spagnoli FM, Brivanlou AH, Massagué J (2007) Balancing BMP signaling through integrated inputs into the Smad1 linker. *Mol Cell* 25(3):441–454.
27. Streit A, et al. (1998) Chordin regulates primitive streak development and the stability of induced neural cells, but is not sufficient for neural induction in the chick embryo. *Development* 125(3):507–519.
28. Stuhlmiller TJ, García-Castro MI (2012) FGF/MAPK signaling is required in the gastrula epiblast for avian neural crest induction. *Development* 139(2):289–300.
29. Cunningham NS, Paralkar V, Reddi AH (1992) Osteogenin and recombinant bone morphogenetic protein 2B are chemotactic for human monocytes and stimulate transforming growth factor beta 1 mRNA expression. *Proc Natl Acad Sci USA* 89(24):11740–11744.
30. Lai TH, Fong YC, Fu WM, Yang RS, Tang CH (2008) Osteoblasts-derived BMP-2 enhances the motility of prostate cancer cells via activation of integrins. *Prostate* 68(12):1341–1353.
31. Augsburger A, Schuchardt A, Hoskins S, Dodd J, Butler S (1999) BMPs as mediators of roof plate repulsion of commissural neurons. *Neuron* 24(1):127–141.
32. Smith KA, et al. (2011) Bmp and nodal independently regulate lefty1 expression to maintain unilateral nodal activity during left-right axis specification in zebrafish. *PLoS Genet* 7(9):e1002289.
33. Lenhart KF, Holtzman NG, Williams JR, Burdine RD (2013) Integration of nodal and BMP signals in the heart requires FoxH1 to create left-right differences in cell migration rates that direct cardiac asymmetry. *PLoS Genet* 9(1):e1003109.
34. Veerkamp J, et al. (2013) Unilateral dampening of Bmp activity by nodal generates cardiac left-right asymmetry. *Dev Cell* 24(6):660–667.
35. Gao B, et al. (2011) Wnt signaling gradients establish planar cell polarity by inducing Vangl2 phosphorylation through Ror2. *Dev Cell* 20(2):163–176.
36. Bartscherer K, Boutros M (2008) Regulation of Wnt protein secretion and its role in gradient formation. *EMBO Rep* 9(10):977–982.
37. Mulligan KA, et al. (2012) Secreted Wingless-interacting molecule (Swim) promotes long-range signaling by maintaining Wingless solubility. *Proc Natl Acad Sci USA* 109(2):370–377.
38. Baeg GH, Selva EM, Goodman RM, Dasgupta R, Perrimon N (2004) The Wingless morphogen gradient is established by the cooperative action of Frizzled and Heparan Sulfate Proteoglycan receptors. *Dev Biol* 276(1):89–100.
39. Sieber C, Kopf J, Hiepen C, Knaus P (2009) Recent advances in BMP receptor signaling. *Cytokine Growth Factor Rev* 20(5-6):343–355.
40. Gamell C, et al. (2008) BMP2 induction of actin cytoskeleton reorganization and cell migration requires PI3-kinase and Cdc42 activity. *J Cell Sci* 121(Pt 23):3960–3970.
41. Foletta VC, et al. (2003) Direct signaling by the BMP type II receptor via the cytoskeletal regulator LIMK1. *J Cell Biol* 162(6):1089–1098.
42. Lee-Hoeflich ST, et al. (2004) Activation of LIMK1 by binding to the BMP receptor, BMPRII, regulates BMP-dependent dendritogenesis. *EMBO J* 23(24):4792–4801.
43. Ridley AJ, et al. (2003) Cell migration: Integrating signals from front to back. *Science* 302(5651):1704–1709.
44. Alarcón C, et al. (2009) Nuclear CDKs drive Smad transcriptional activation and turnover in BMP and TGF-beta pathways. *Cell* 139(4):757–769.
45. Steinfeld J, et al. (2013) RPE specification in the chick is mediated by surface ectoderm-derived BMP and Wnt signalling. *Development* 140(24):4959–4969.
46. Hamburger V, Hamilton HL (1992) A series of normal stages in the development of the chick embryo. 1951. *Dev Dyn* 195(4):231–272.
47. Chapman SC, Collignon J, Schoenwolf GC, Lumsden A (2001) Improved method for chick whole-embryo culture using a filter paper carrier. *Dev Dyn* 220(3):284–289.
48. Song J, Yue Q, Münsterberg A (2011) Time-lapse imaging of chick cardiac precursor cells. Cell Migration, Developmental Methods and Protocols. *Methods in Molecular Biology*, eds Wells CM, Parsons M (Humana Press, New York), Vol 769, pp 359–372.

Supporting Information

Song et al. 10.1073/pnas.1321764111

SI Materials and Methods

Embryo Culture, Manipulations, and ex Vivo Migration Assay. Fertile brown eggs (Henry Stewart) were incubated at 38 °C for 12–13 h in a humidified incubator. After embryos had reached appropriate stages, easy culture (EC) was prepared as described (1). Electroporation, grafting, and ex-vivo migration essays were carried out as described previously (2–4). All manipulations were done at Hamburger Hamilton (HH) stage 3; however, in most cases, embryos were mounted for video microscopy once they had reached HH4. Thus, healthy embryos could be selected. Heparin beads (Sigma, H5263) were incubated with bone morphogenetic protein (BMP) 2 (200 μg/mL; R&D systems) or BSA (Promega) for 1 h before implantation, transferred with forceps to the ventral sides of host embryos, and implanted into the future heart-forming region. Activity of recombinant BMP2 was tested by induction of ectopic expression of the homeobox transcription factor Nkx2.5, as shown by Schlange (5).

Long-term Video Microscopy. Embryos cultured in six-well cell culture plates (Falcon) were time-lapse-imaged on an inverted wide-field microscope (Axiovert; Zeiss). Brightfield and fluorescent images were captured at 2.5× 0.63 magnification every 6 min for 20–24 h, using Axiovision software. Images were collected using Axiovision autofocus and an Axiocam MRm camera. After ∼24 h, most embryos had reached stage HH9 to HH10; healthy-looking embryos were included in the analyses.

Two-Photon Microscopy for pSmad Imaging. Heparin beads (Sigma, H5263) were incubated with BMP2 (200 μg/mL; R&D systems) or BSA (Promega) for 1 h before implantation. To create Wnt3a cell pellets, cells were seeded onto culture plates 24 h before implantation. Pellets and beads were implanted into HH5 embryos, left at 30 °C for 30 min and at 37 °C for 3 h. Samples were then fixed using paraformaldehyde and immune-labeled using phospho-SMA and MAD related protein (pSmad) primary antibody, Alexa 488 secondary, and then mounted between slides and coverslips. Images were taken using a TriM Scope II multiphoton microscope (LaVision BioTec). Eighty 0.72-μm slices were recorded at 880-nm wavelength, using a 20× objective, and 4–7% laser power, increasing exponentially. Power at the objective was measured at 48 mW, increasing to 73 mW. Images were analyzed by integrating the pixel intensity for concentric rings moving out from the center of the bead. We noticed variation of pixel intensity around the beads ($n = 6$); however, this was not consistently found on the same side. Thus, there was no evidence for a difference in competence of the mesoderm to respond to the signal.

Image Analysis. Automated fluorescent cell tracking was done using Optimas VI or Image-Pro (MediaCybernetics) software, as described (2–4). To quantify the effects observed, we measured the distance of GFP-labeled cardiac progenitor cells (CPCs) from the midline at the level of the forming heart at HH9, using Axiovision (Carl Zeiss), and confirmed statistical significance using Student t test ($P < 0.05$).

Early-stage Tracking. Fluorescent channel images were fluorescence background-corrected, using a photobleaching compensation plugin (Andor iQ 2.5), by using reference fluorescence (i.e., fluorescence not from CPCs). Next, images were corrected for background tissue movement, using a custom-written plugin (Image-Pro analyzer 7). Finally, the threshold for the images was set individually, using a histogram-based method, and subsequently tracked (Image-Pro analyzer 7). For angle determination, the angle of each Cartesian coordinate for each time was calculated from the midline of the image, and the mean track angle was determined from the first 10 coordinates. All track angles were collated in a histogram (20° bin sizes), transformed to radians, and plotted as compass plots (Matlab 2012b; Mathworks).

Line profiles and intensity profiles were calculated using Image J. For line profiles, a circle 100 μm wide was drawn around the bead, and a z axis profile was plotted in Image J. Intensity profiles were determined by first averaging 30 (mesoderm) slices and then using the radial plot function to calculate the intensity change moving out from the bead.

Plasmid Constructs and in Situ Hybridization. Expression constructs were generated in the chicken β-actin promoter-internal ribosomal entry site-GFP vector, which contains the chicken β-actin promoter and an internal ribosomal entry site upstream of GFP. All primers used included restriction sites for molecular cloning. Sequences encoding HA-tag were added in either forward or reverse primers. Constitutively active receptor mutants of human activin-like kinase 3 (ALK3; Q233D) and mouse activin-like kinase 6 (Alk6; Q203D) were kindly provided by Andrew Chantry (University of East Anglia, Norwich). The constitutively active human SMAD1-EVE, in which the carboxy-terminal phosphorylation site was altered from Ser-Val-Ser to Glu-Val-Glu, and the GSK3β resistant mutant, SMAD1-GM, in which the GSK3β phosphorylation sites were mutated, were generous gifts from Eddie DeRobertis (University of California, Los Angeles) and are described in ref. 6. Wnt3a and dnWnt3a plasmids were described previously, and all plasmids were prepared for electroporation, as reported in ref. 2). Primer sequences were as follows:

cBmp2F+XbaI: TCTAGAATGGTTGCCGCCACCCGCTCCCTC;

cBmp2R+Not1HA:GCGGCCGCTCAAGCGTAATCTGGAACATCGTATGGGTATCAGCGGCACCCGCAGCCC;

cBmp4 F+XbaI: TCTAGAATGATTCCTGGTAACCGAATGC;

cBmp4R+NotIHA:GCGGCCGCTCAAGCGTAATCTGGAACATCGTATGGGTAGCGGCACCCGCACCCCTCCA;

dnhALK3F+XbaI: TCTAGAATGGCTCAGCTATACATTTACATCA;

dnhALK3R+NotIFLAG:GCGGCCGCCTACTTGTCATCGTCGTCCTTGTAATCAACTGGAATAAATGCTTCAT;

dnmAlk6F+XbaI: TCTAGAATGCTCTTACGAA GCTCTGGAAAATT;

dnmAlk6R+NotIFLAG:GCGGCCGCCTACTTGTCATCGTCGTCCTTGTAATCGTCTCTCAGGGACTCTCCA;

cAlk3-F: ATGACTCGACTGAGAGTTTGTG AGC;

cAlk3-R: TCAAATCTTTACATCTTGTGATTCC;

cAlk6-F: ATGCCCTTGCTTAGCTCCAGCAAGT;

cAlk6-R: TCAGAGCTTAATGTCCTGCGACTCT;

cSmad1F+XbaIHA:TCTAGAATGTACCCATACGATGTTCCAGATTACGCTAACGTGACAAGTTTATTTTCCT; and

cSmad1R+NotI: GCGGCCGCTTAAGACACTGAAGAAATAGGA.

We amplified chick BMP2 and BMP4 from day 2 embryo cDNA for probe preparation and gene expression experiments. Thomas Schultheiss (Rappaport Institute, Haifa, Israel) provided probes for ventricular myosin heavy chain (vMHC) and the homeodomain transcription factor Nkx2.5 probes. In situ hybridization followed standard protocols (7).

Cryosections and Immunochemistry. Embryos were embedded in optimal cutting temperature (OCt) compound (Tissuetek) and sectioned at 10 μm thickness on a Leica CM1900 cryostat. Immunochemistry was performed as described (1), using rabbit anti-GFP (Abcam, 1:500) and mouse anti-rabbit-Alexa488 (green, 1:1,000).

1. Chapman SC, Collignon J, Schoenwolf GC, Lumsden A (2001) Improved method for chick whole-embryo culture using a filter paper carrier. *Dev Dyn* 220(3):284–289.
2. Yue Q, Wagstaff L, Yang X, Weijer C, Münsterberg A (2008) Wnt3a-mediated chemorepulsion controls movement patterns of cardiac progenitors and requires RhoA function. *Development* 135(6):1029–1037.
3. Yang X, Dormann D, Münsterberg AE, Weijer CJ (2002) Cell movement patterns during gastrulation in the chick are controlled by positive and negative chemotaxis mediated by FGF4 and FGF8. *Dev Cell* 3(3):425–437.
4. Song J, Yue Q, Münsterberg A (2011) *Time-lapse imaging of chick cardiac precursor cells. Cell Migration, Developmental Methods and Protocols.* Methods in Molecular Biology, eds Wells CM, Parsons M (Humana Press, New York), Vol 769, pp 359–372.
5. Schlange T, Andrée B, Arnold HH, Brand T (2000) BMP2 is required for early heart development during a distinct time period. *Mech Dev* 91(1-2):259–270.
6. Fuentealba LC, et al. (2007) Integrating patterning signals: Wnt/GSK3 regulates the duration of the BMP/Smad1 signal. *Cell* 131(5):980–993.
7. Schmidt M, Patterson M, Farrell E, Münsterberg A (2004) Dynamic expression of Lef/Tcf family members and beta-catenin during chick gastrulation, neurulation, and early limb development. *Dev Dyn* 229(3):703–707.
8. Minko K, Bollerot K, Drevon C, Hallais MF, Jaffredo T. (2003) From mesoderm to blood islands: patterns of key molecules during yolk sac erythropoiesis. *Gene Expr Patterns* 3(3):261–272.

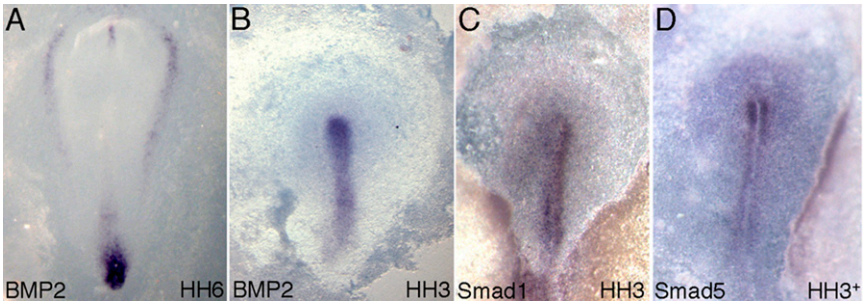

Fig. S1. BMP2 and downstream effectors Smad1 and Smad5 are expressed in the primitive streak at HH3-3^{+}, when CPCs ingress. (*A*) In situ hybridization of BMP2 at HH6 in primitive streak and lateral regions flanking migrating CPCs, and (*B*) at HH3 in primitive streak. (*C*) In situ hybridization of Smad1 at HH3 and (*D*) Smad 5 at HH3^{+}.

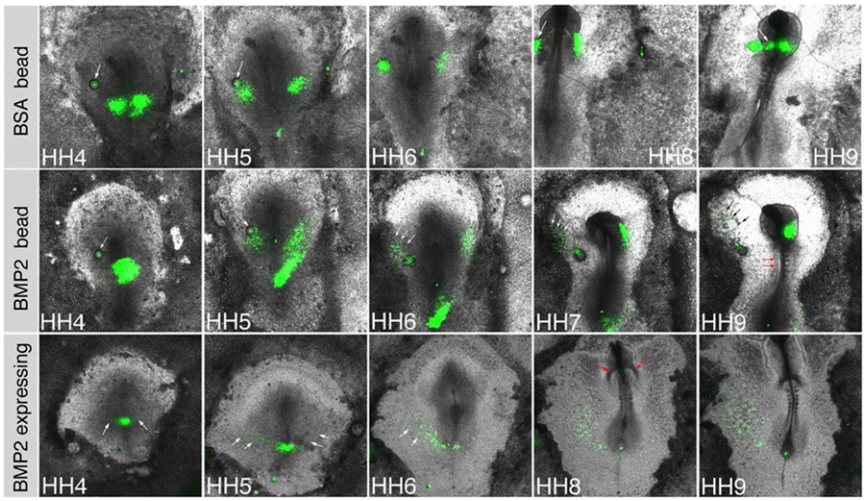

Fig. S2. BMP2 beads or expression of BMP2 leads to displacement of cells. White-light images overlaid with GFP migrating cells at different stages of development. GFP-expressing CPCs reach the primary heart tube after implanting a BSA bead. A BMP2 bead prevents cells from reaching the primary heart tube on the bead side. Note that the paraxial mesoderm fails to form epithelial somites on the bead side (red arrows), indicative of elevated BMP2 levels. CPCs expressing BMP2-GFP are displaced widely. Overall morphology and development is similar in all embryos: the axis develops and the anterior intestinal portal and primary heart tube forms.

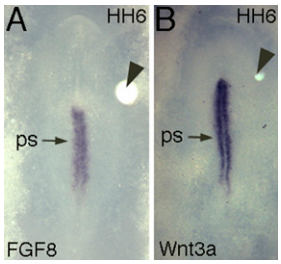

Fig. S3. BMP2 does not induce ectopic expression of Wnt3a or fibroblast growth factor (FGF) 8. (*A*) Endogenous expression of FGF8 and (*B*) Wnt3a transcripts after BMP2 bead implantation; no ectopic expression was detected (black arrowheads). We previously demonstrated that Wnt3a affects CPC migration (2). In addition, FGF8 controls the migration of mesoderm progenitors emerging from the primitive streak at midgastrulation (3). Therefore, to exclude the possibility that high levels of BMPs induced ectopic expression of Wnt3a or FGF8, a BMP2-bead was implanted close to the HH3 primitive streak in the migration path of CPCs. Embryos were harvested at HH5 and HH6, and Wnt3a and FGF8 expression was assessed by in situ hybridization. Transcripts for Wnt3a and FGF8 were detected in the normal patterns, but BMP2 beads did not lead to ectopic expression.

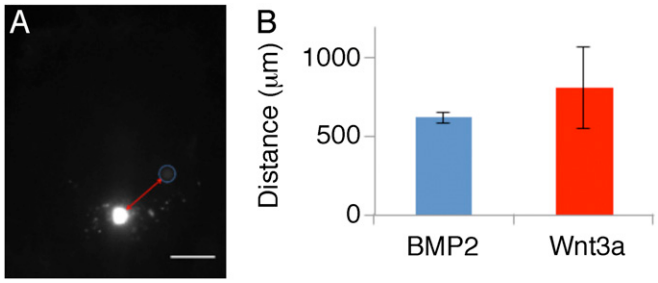

Fig. S4. Initial BMP2 bead or Wnt3a pellet placement is not different. (*A*) Initial distance of BMP2 beads and Wnt3a pellets from CPCs, measured (indicated by red arrow) from the edge of the grafted cells to the edge of the bead (blue). (Scale bar, 500 μm.) (*B*) Distances measured for BMP2 ($n = 12$) and Wnt3a ($n = 4$). Errors are standard deviation. It could be possible that the strong, bilateral effects that we see for the Wnt3a pellet compared with the BMP2-coated bead are a result of the Wnt3a pellet being grafted closer to the CPCs at HH3+. To test this, we measured the shortest distance from the edge of the CPC region to the closest edge of the cell pellet (or bead). We found no difference in distance from the CPC cluster for either the bead or the pellet.

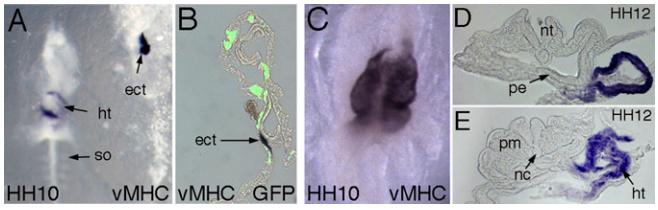

Fig. S5. (*A* and *B*) Expression of vMHC transcripts (purple) was detected in embryos overexpressing BMP2, illustrating that displaced prospective cardiac cells are still correctly specified. (*A*) Whole-mount (*B*) section; anti-GFP antibody (green) detects transfected CPCs. (*C*) Example of primary heart tube expressing the differentiation marker vMHC in a HH10 embryo overexpressing BMP2 in CPCs. (*D* and *E*) Sections of a HH12 embryo overexpressing BMP2 in CPCs show normal morphology of neural tube (nt), notochord (nc), paraxial mesoderm (pm), pharyngeal endoderm (pe), and the forming heart (ht), which expresses vMHC (purple).

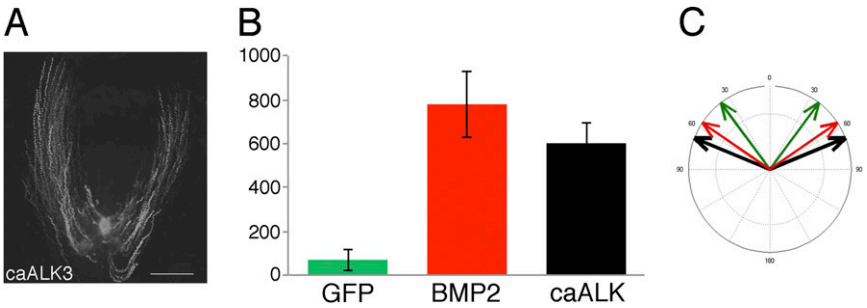

Fig. S6. Electroporation of constitutively active activin-like kinase (caALK) expression plasmids into CPCs. (*A*) Migration trajectories of constitutively active receptors. (Scale bar, 500 μm.) These trajectories resulted in (*B*) lateral displacement at HH10 (center, 602 ± 90 μm). (*C*) Exit trajectories were wide (68° ± 3°); errors are standard error of the mean, denoted by the width of the arrows. Constitutively active experiments are a combination of both ALK3 and ALK6, with both BMP2 and GFP data shown for comparison.

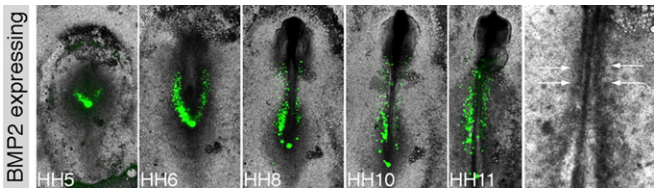

Fig. S7. BMP2 overexpression in prospective paraxial mesoderm cells has no effect on their migration trajectories or their final position but does prevent epithelialization of somites, as shown in higher magnification at HH11 (white arrows). This suggests that BMB2 does not alter migration patterns of all mesoderm progenitors. White-light images are overlaid with GFP tracks, and different developmental stages are shown.

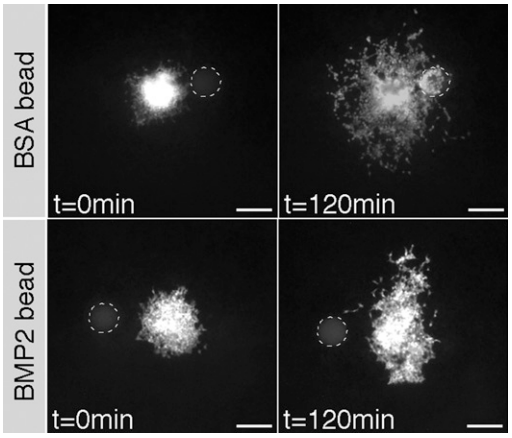

Fig. S8. GFP-labeled HH3 primitive streak cells from prospective cardiac regions were exposed ex vivo to BSA or BMP2 beads. Time-lapse recordings were taken (Movie S1, still images are shown at different times). CPCs are highly motile and migrate away from the explant in all directions (*Upper*), but cells avoid the vicinity of a BMP2 bead (*Lower*; Movie S2).

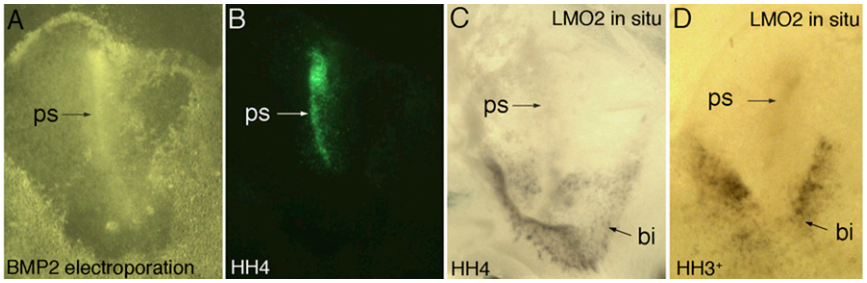

Fig. S9. BMP2 overexpression in HH3 primitive streak does not induce the early blood island marker, LIM-domain only transcription factor 2 (LMO2). (*A*) White-light image of HH4 embryo, 5–6 h after electroporation of (*B*) BMP2-GFP into the primitive streak, including CPCs. (*B*) Example of LMO2 expression in a $HH3^{+}$ stage embryo overexpressing BMP2 in the primitive streak ($n = 4$). (*C*) In situ hybridization shows LMO2 in blood islands (bi), but not in the primitive streak. Embryo in *C* was slightly folded after in situ procedure. (*D*) Another example of a treated embryo, labeled by in situ hybridization with a probe for LMO2 is shown. This embryo is slightly younger than the one shown in *A*–*C* and remained flat during fixation. For LMO2 expression, see ref. 8 and http://geisha.arizona.edu/geisha/search.jsp?entrez_gene=455716.

Table S1. Exit trajectories

Embryo manipulation	n	Tracks	Angle from midline			
			Left	Right	Mean (σ)	Error ($\sigma/\sqrt{n}$)
GFP_wt	5	115	35	38	37	2
BMP2	12	223	59	52	56	2
caALK_combined	8	133	67	69	68	3
SMAD1	8	103	43	40	42	2
SMAD1_EVE	6	93	56	62	59	3
SMAD1_GM	7	129	52	47	50	4
dnGSK3β	8	83	52	53	53	4
GFP+Wnt3a	4	93	60	64	62	3
dnWnt3a+BMP2	6	72	42	38	40	3
GSK3β+Wnt3a	6	116	—	—	42	2
GSK3β+BMP2	6	133	—	—	36	2
GFP_BMP2_bead	10	117	—	—	41	2
BMP4	8	126	55	50	53	3

Average angles over first 60 min after exiting the streak. ALK, activin-like kinase; ca, constitutively active; dn, dominant negative; EVE, Glu-Val-Glu; GSK, glycogen synthase kinase; wt, wild-type.

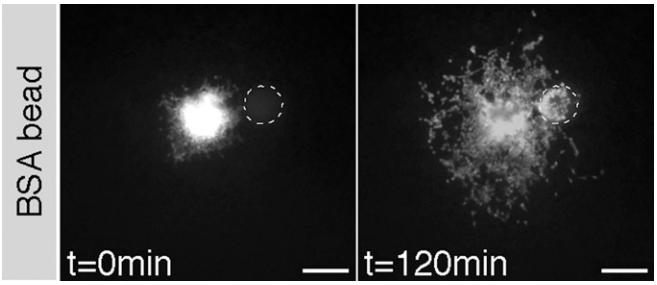

Movie S1. Time-lapse recording of prospective cardiac cells from HH3 primitive streak, challenged with a BSA control bead in explant culture, as described previously (2). Cells migrate radially away from the explant. Stills are shown in Fig. S8.

Movie S1

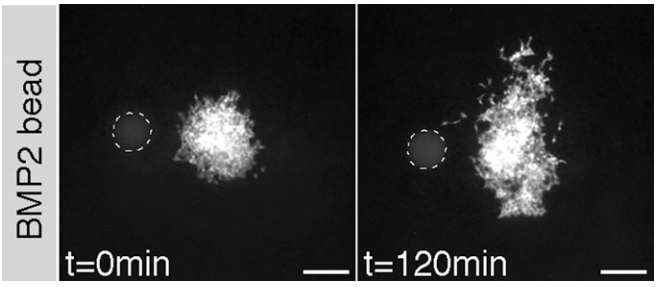

Movie S2. Time-lapse recording of prospective cardiac cells from HH3 primitive streak, challenged with a BMP2-soaked bead in explant culture, as described previously (2). Cells migrate from the explant to avoid the bead. Stills are shown in Fig. S8.

Movie S2